2025 16th Annual Power Electronics & Drives: Systems and Technologies Conference (PEDSTC) 4-6 February 2025, University of Tabriz, Tabriz, Iran

Implementation of a Global Characteristic Scan Mechanism Integrated with the Perturb & Observe MPPT Algorithm under Partial Shading Conditions

Soheil Hasani Sangani
Department of ECE
Tarbiat Modares University
Tehran, Iran
0000-0003-4809-2074

Mohamad Reza Moslemnejad
Department of R&D
Behine-Sazan-Toos Company
Mashhad, Iran
moslemnezhad-m@bst.co.ir

Mojtaba Saeedi
Department of R&D
Behine-Sazan-Toos Company
Mashhad, Iran
saeedi-m@bst.co.ir

Alireza Jalalitalab
Department of R&D
Behine-Sazan-Toos Company
Mashhad, Iran
jalalitalab-a@bst.co.ir

Reza Beiranvand
Department of ECE
Tarbiat Modares University
Tehran, Iran
0000-0002-3214-7563

***Abstract*—Maximum power point tracking (MPPT) is considered a high priority feature for grid-tied solar inverter systems. Various MPPT algorithms are able to identify a local maximum power point (LMPP) on the P-V curve of a photovoltaic (PV) panel. Nonetheless, they often stop scanning the characteristic as soon as they detect the first available maximum. This would be problematic in situations where the characteristic possesses several maxima due to partial shading. Under such conditions, the employed MPP tracker needs to scan the P-V curve to locate the global maximum power point (GMPP) and ensure the system operates at that point. However, it is not recommended for MPPT algorithms to scan the entire P-V curve owing to efficiency and dissipation issues, unless absolutely necessary. Thus, it is crucial to provide a strategy that can identify the region containing the GMPP, and then let the LMPP tracker locate the exact GMPP. This paper investigates a proper global characteristic scan mechanism (GCSM) that incorporates the perturb & observe (P&O) algorithm to accurately identify the GMPP. The proposed algorithm is applied on a single-phase grid-tied solar inverter system operating at 20 kHz under varying input power conditions. Eventually, the experimental results are presented to confirm the appropriate performance of the system.**

Keywords—Maximum power point tracking (MPPT), Partial shading condition (PSC), grid-tied solar inverter, global characteristic scan mechanism (GCSM)

I. INTRODUCTION

Renewable energy sources, such as PV panels and wind turbines, are becoming widespread owing to the catastrophic environmental issues emerged by fossil fuels [1]. PV panels are one of the most favorable types of the mentioned energy sources, due to their long lifespan and convenient maintenance, and they are manufactured for residential, commercial, and large-scale use [2, 3]. However, there are considerations employing solar panels that must be dealt with, encompassing lack of uniform irradiance and partial shading [4]. Although bypass diodes, which are installed in typical PV panels, provide protection against hotspots, they also introduce multiple maxima in the panels' characteristics [5].

Partial shading condition (PSC) occurs only when a range of panels are connected in series or series-parallel configurations. Therefore, lack of uniform irradiance or PSC do not result in multiple maxima in a purely parallel connection. Nevertheless, such a connection does not seem appropriate for solar inverter systems due to the subsequent remarkably high input current values bringing about cost issues. Thus, to manage current stresses on input components, a purely parallel connection is not recommended [6]. Partial shading condition might be caused by various factors, including buildings, trees, and soiling effect [7]. Consequently, due to the inevitable presence of series-connected PV panels in most occasions, it seems necessary to integrate a proper characteristic scan strategy with the local maximum power point tracker.

There is a variety of methods proposed in numerous journals to deal with PSC. For instance, [8] and [9] employ the gray wolf optimization (GWO) technique, which was originally introduced in [10], to locate the GMPP. Contrary to [8], utilizing only a GWO technique, [9] integrates it with the perturb & observe (P&O) algorithm to pinpoint the exact location of the GMPP within a particular area suggested by the GWO strategy. Although [9] has successfully managed to reduce the computational burden compared to [8], all GWO-based methods are not desirable in terms of the volume of arithmetic operations. In general, it is more effective to combine a curve scanner with an LMPP tracker, such as P&O or incremental conductance (IC) algorithms. An improved MPPT controller utilizing P&O algorithm is proposed in [11]. In spite of the thorough analysis it provides to explain the behavior of both shaded and unshaded panels belonging to a single string under PSC, it possesses a major drawback. Specifically, the provided method in [11] requires a separate voltage sensor for each panel, leading to cost increase and more complex installation. Furthermore, a modified IC algorithm applicable for PSC is presented in [12]. Although it has been able to refine the transient response of a traditional IC algorithm, its application in grid-tied solar inverter systems has not been investigated.

Various mathematical approaches, known as extremum seeking control (ESC), are proposed in [13] and [14]. Initially, [13] provides a comprehensive analysis for series-connected PV panels under PSC. Afterwards, it presents an MPPT

979-8-3315-3394-6/25/$31.00 ©2025 IEEE

algorithm involving digital filter implementation leading to narrow searching regions. Additionally, [14] explores an improved ESC algorithm that significantly minimizes output power oscillations compared to conventional ESC-based methods. Despite the reliability and efficiency of these methods, they require considerable calculations in addition to the fact that they have not been applied to grid-tied systems for performance evaluation. Furthermore, some other nature-inspired strategies, similar to GWO, are addressed in [15] comprising firefly algorithm, ant colony optimization, artificial bee colony based algorithm and so on.

The proposed GCSM of the present paper, which will be discussed in the following sections, is inspired by the findings provided in [16] and [17], Particularly a claim made in [17] stating that the location of the GMPP is not entirely random. In fact, the values corresponding to LMPPs experience a gradual increase toward the GMPP, and then drop slowly. Nevertheless, there are situations where the mentioned rule no longer applies. For example, [18] - [20] present some solar P-V characteristic curves comprising GMPPs appeared at the far left of the voltage axis. However, there are several reasons why it is unnecessary for the system to scan these types of GMPPs. First, they usually appear below the normal input voltage values of typical residential solar inverter systems, which is 70 volts for the system under study. Second, they are surrounded by some LMPPs with values very close to that of the GMPP. Therefore, it would not make a significant difference for the system to operate at the exact GMPP or at an LMPP with approximately the same power value.

Section II provides a detailed description of the solar inverter system under study. Then, section III presents the empirical results of the system under various conditions. Eventually, a conclusion is provided in section IV.

II. Solar Inverter System

A. Power Section

Fig. 1 depicts the circuit diagram of a typical grid-tied solar inverter system. The entire process of harnessing the energy received from the sun, and making it suitable for grid injection is carried out by such a system. The power section of the employed solar inverter consists of three major stages, including a boost converter, a highly efficient and reliable inverter concept (HERIC) inverter, and an LCL filter. Firstly, the boost converter is responsible for locating the maximum power point of the panel using the MPPT algorithm when the input voltage is below 400 volts. Secondly, the HEIRC inverter and LCL filter convert the received DC energy from the previous stage into AC current, synchronized with the grid and proportional to the input irradiance. Furthermore, they maintain the DC bus voltage on 400 volts through a cascaded loop structure, as long as the input voltage is below 400 volts. On the other hand, when the input voltage exceeds 400 volts, the boost converter is disabled, and the inverter stage handles maximum power point tracking, too.

B. Control Section

Solar inverters require complex control structures involving multiple compensators, as shown in Fig. 1. It is highly recommended to implement a voltage regulator on the panel voltage utilizing a proportional-integral (PI) controller. This allows the panel voltage to be used as the control parameter for MPPT to scan the characteristic curve. Panel voltage is preferable over the duty cycle for this purpose in terms of the overall stability of the system. Thus, the boost converter is controlled by a PI compensator receiving its reference voltage from the MPPT algorithm.

In the inverter stage, a cascaded loop structure is utilized to shape the grid current, while the bus voltage is maintained. Initially, a phase-locked loop (PLL) block derives the phase and frequency of the utility grid, which are necessary to generate the grid reference current. Then, a proportional-resonance (PR) controller, fed by the difference between the reference and actual current values, adjusts the current injected into the grid. Meanwhile, the outer loop of the cascaded structure determines the amplitude of the reference current to regulate the bus voltage at 400 volts. However, when the input voltage exceeds 400 volts, the outer loop also participates in maximum power point tracking, compensating for the absence of boost converter operation. It is worth noting that in order to enhance the harmonic profile of the current injected into the grid, the PR controller can be combined with harmonic compensators. In this paper, a pair of harmonic compensators tuned to the third and seventh harmonic frequencies are added to the main PR controller. The s-domain transfer function of the current controller is provided in equation (1).

$$H_{PR}(s) = k_p + \sum_{h=1,3,7} \frac{k_h \omega_c s}{s^2 + 2\omega_c s + (h\omega_r)^2}. \quad (1)$$

III. Partial Shading Condition and the Proposed MPPT Algorithm

A. Partial Shading Condition

Partial shading can be caused by several factors, such as buildings, trees, clouds, or any obstruction between the sun's irradiation and the solar panels. PSC can be described as non-

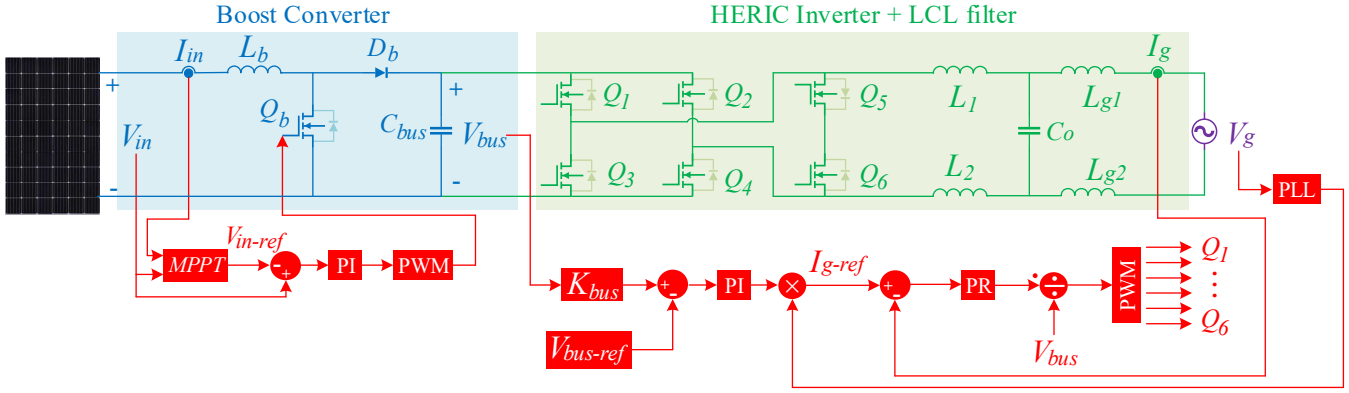

Fig. 1. Circuit diagram of the employed single-phase grid-tied solar inverter system.

uniform irradiance across different solar panels within a string. In such situations, the current of the entire string is limited by the panel receiving the least irradiance. However, as shown in Fig. 2, PV panels are typically equipped with bypass diodes to exclude the shaded panels from the circuit. Nevertheless, these diodes modify the I-V and P-V characteristics of the string.

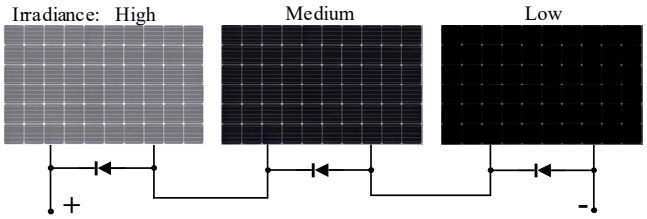

Fig. 2. Series-connected PV panels under PSC.

Fig. 3 represents the I-V characteristic of the string from Fig. 2 in the presence of bypass diodes. Under non-uniform irradiance, the saturation current for each panel depends on the amount of irradiance it absorbs. Therefore, the I-V curve shown in Fig. 3 can result in various P-V curves, in terms of the distribution pattern of LMPPs. Additionally, Fig. 3 includes two P-V curves derived from the I-V curve, with different GMPP locations relative to the LMPPs. In such conditions, MPPT algorithms must be equipped with proper additional strategies to pinpoint the GMPP.

B. Description of the Proposed GCSM

It has been observed that the GMPP does not happen to be placed somewhere between LMPPs in a sheer random manner. Instead, starting from the open-circuit voltage, the LMPPs increase before gradually decreasing at lower voltage values. This behavior forms the basis of the proposed scan mechanism for the P-V characteristic, which is designed to locate the GMPP by incorporating the P&O algorithm.

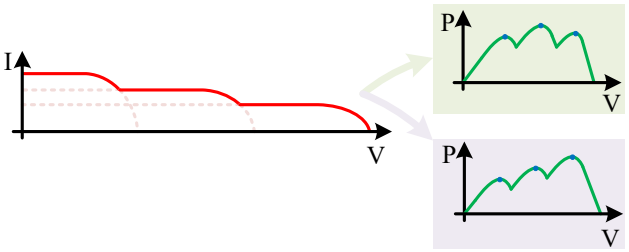

Fig. 3. P-V and I-V curves corresponding the string of Fig. 2.

Fig. 4 presents a depiction of a flowchart representing the proposed GCSM. This mechanism is based on the pattern mentioned in the previous paragraph in addition to what [16] states claiming that the MPP occurs at 76% of the open circuit voltage for a single PV panel. Therefore, the GCSM first inspects the power values corresponding to the LMPPs, expressed as $V_{LMPP}(n)$, then identifies the region containing the GMPP, and finally allows the P&O algorithm to pinpoint the exact location of the GMPP. The value of $V_{LMPP}(n)$ can be expressed as:

$$V_{LMPP}(n) = 0.76 \times V_{oc}\left(\frac{N-n}{N}\right). \qquad (2)$$

Where V_{oc} is the open circuit voltage, N is the number of PV panels in a string, and n ranges from 0 to $N-1$. It is worth noting that the GCSM is only triggered when the PSC_FLAG is set, which occurs when a significant power change is detected. Additionally, the PSC_FLAG must be forced to unity at regular intervals, even in the absence of significant power changes.

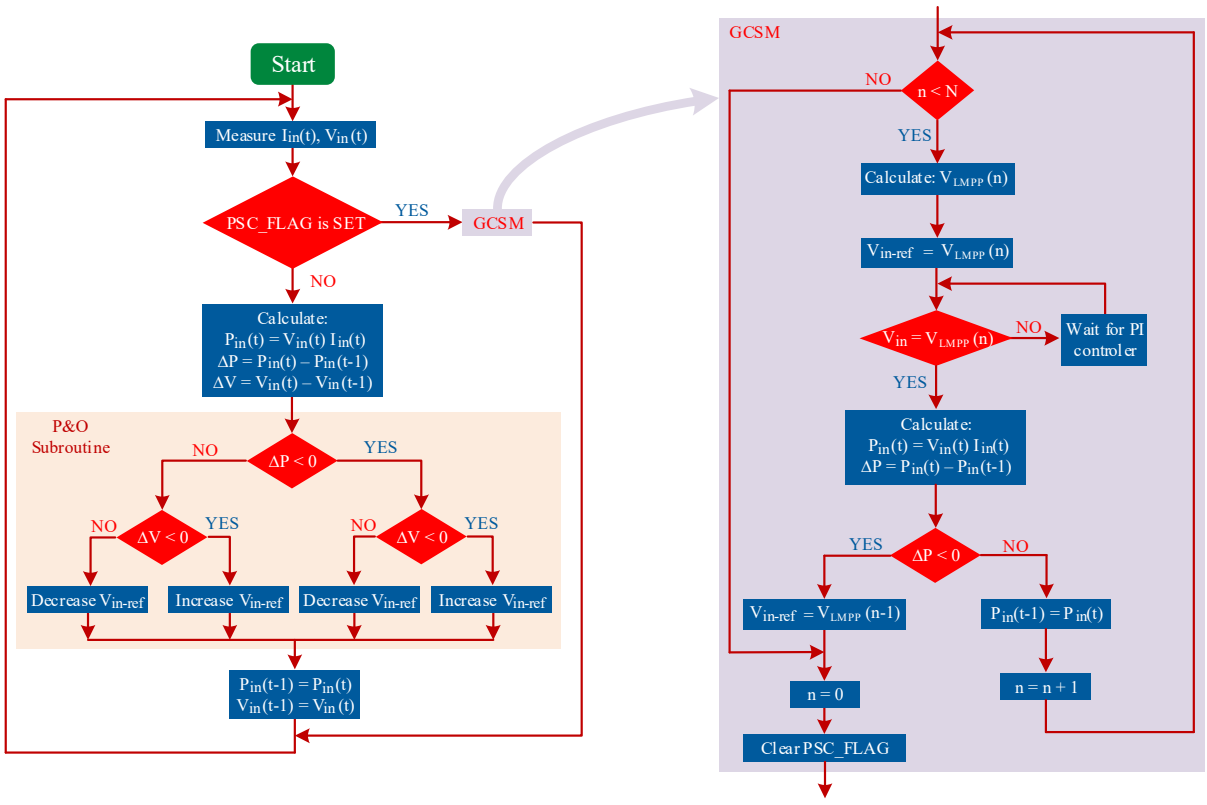

Fig. 4. The proposed GCSM combined with a P&O MPPT algorithm

IV. Experimental Validation

This section presents the experimental results of the proposed GCSM, incorporating a P&O algorithm, applied to a grid-tied solar inverter system. PSC is simulated by covering some panels in the string, as shown in Fig. 5. The control unit of the overall system is depicted in Fig. 1, consisting of a cascaded loop structure for the inverter stage and an MPPT controller for the DC-DC stage. The cascaded loop structure includes an inner loop to shape the current injected into the grid and an outer loop to regulate the DC bus voltage, which determines the amplitude of the grid current. It is important to note that a PI controller is responsible for regulating the panel voltage to $V_{LMPP}(n)$, where n increases from 0 to $N-1$. However, this PI controller does not jump directly from, for example, $V_{LMPP}(n_0)$ to $V_{LMPP}(n_0+1)$; Instead, it adjusts the panel voltage smoothly in predetermined steps. Furthermore, the delay between these steps can be fine-tuned based on stability requirements and the desired transient response of the system.

Table I. Specifications of the Solar Inverter System

	Parameter Description	Symbol	Value
Boost converter	Inductor	L_b	$1\ mH$
	Capacitor	C_{bus}	$5 \times 470\ \mu F$
	PI Proportional Gain	k_P	0.1
	PI Integral Gain	k_I	10
	Switching Frequency	f_s	$20\ kHz$
Inverter Stage	Output Inductors	L_1, L_2	$500\ \mu H$
	Output Capacitor	C_o	$10\mu F$
	DC Bus Reference Voltage	$V_{bus-ref}$	4
	DC Bus Feedback Ratio	k_{bus}	0.01
	PI Proportional Gain	k_P	20
	PI Integral Gain	k_I	100
	PR Cut-off Frequency	ω_c	$5\ rad/sec$
	PR Resonance Frequency	ω_r	$50\ rad/sec$
	PR Proportional Gain	k_P	5
	PR Resonance Gains	$k_h(h=1)$	4000
		$k_h(h=3)$	100
		$k_h(h=7)$	100
	Switching Frequency	f_s	$20\ kHz$
Grid	Grid Inductors	L_{g1}, L_{g2}	$1.8\ mH$
	Grid Voltage (RMS)	V_g	$220\ V$
	Grid frequency	f_g	$50\ Hz$
Solar panels	Open Circuit Voltage	V_{OC}	$46.41\ V$
	Short Circuit Current	I_{SC}	$8.14\ A$
	Number of series-connected Panels	-	9

Fig. 5. A string of solar panels under PSC.

Fig. 6 shows the implemented grid-tied solar inverter system, including its power and control circuitries. The control unit employs a TI-C2000 microcontroller module, TMS320F28335, to implement all the compensators shown in Fig. 1. Table I lists the specifications of the system under study, including the values of controller gains, inductances, capacitances, and other operational parameters. Before conducting any experiments on the implemented prototype, the system's performance was validated through computer simulations using PSIM software. Therefore, all the component and compensator values mentioned in Table I were verified in the PSIM simulator to ensure the system's reliability and stability.

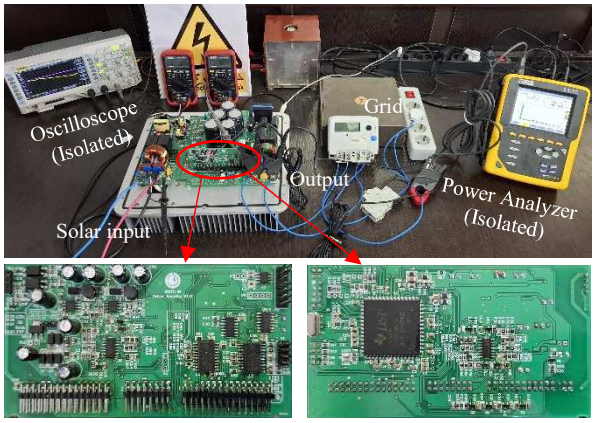

Fig. 6. Implemented grid-tied solar inverter system.

At this point, a string of nine solar panels connected in series can be applied to the inverter system under both uniform and non-uniform irradiance conditions. The specifications of the PV panels used, as well as the utility grid (including its voltage and frequency), are provided in Table I. For instance, Fig. 7 shows the input voltage and DC bus voltage waveforms of the system, demonstrating how the proposed GCSM responds under uniform irradiance. Note that the reference voltage of the PI controller, installed on the input voltage, is updated every $500\ ms$ to facilitate the analysis of the waveforms. However, as indicated in Fig. 7, the suitable performance of the input voltage regulator makes it possible to reduce the reference voltage update interval for the final firmware.

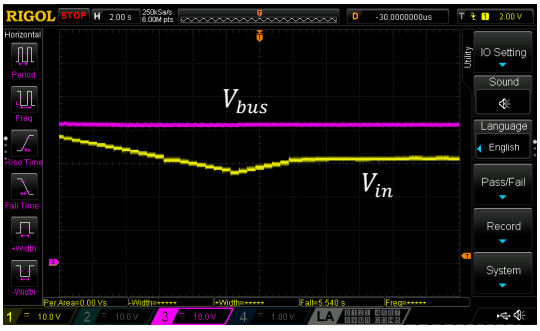

Fig. 7. Input voltage and DC bus voltage waveforms under uniform irradiance for nine series-connected panels producing 2 kW of power.

Under uniform irradiance, as shown in Fig. 7, the proposed GCSM is designed to cease scanning at the first LMPP starting from the open-circuit voltage. According to Fig. 7, the GCSM stops at $V_{in} = 310\ V$, which is approximately $80\ V$ below the open-circuit voltage. Furthermore, the system injects about $2\ kW$ into the grid, resulting in a grid current of $8.5\ A$. Fig. 10 demonstrates the current and voltage waveforms of the grid

under uniform sunlight, whereas Fig. 11 shows the harmonic profile of the grid current.

However, when one or more panels are shaded, as depicted in figures 8 and 9, the situation changes significantly. For instance, Fig. 8 shows a condition where one of the nine panels is completely shaded. It is important to note that, in this paper, a shaded panel refers to one that is covered by a sunlight-blocking object, as shown in Fig. 5. In this scenario, as illustrated in Fig. 8, the proposed GCSM stops scanning at $V_{in} = 285\,V$, indicating that it has skipped the region containing the first local maximum. Furthermore, the power drops by approximately one-ninth compared to the previous case as a result of one panel being bypassed. Similarly, Fig. 9 shows the waveforms when two panels are shaded. In this case, the GCSM halts the scanning process at $V_{in} = 245\,V$, with power decreasing by another one-ninth. From Fig. 9, it can be inferred that the proposed GCSM skipped the first two LMPPs and eventually stopped at the third, as two of the nine panels were shaded.

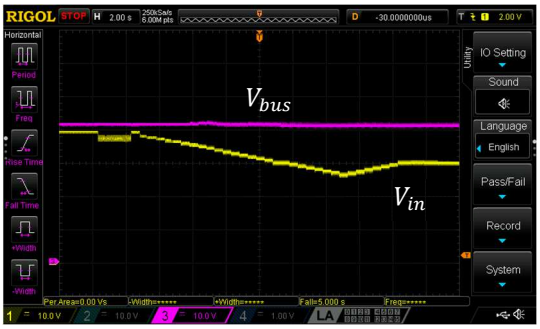

Fig. 8. Input voltage and DC bus voltage waveforms under PSC, for one panel shaded out of nine.

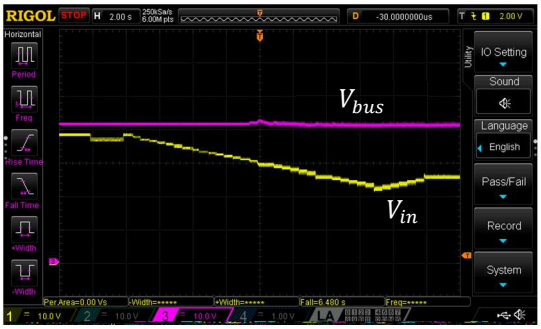

Fig. 9. Input voltage and DC bus voltage waveforms under PSC, for two panels shaded out of nine.

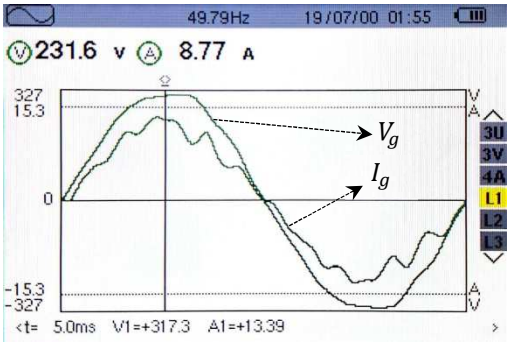

Fig. 9. Voltage and current waveforms of the grid under uniform irradiance.

At this point, some of the grid waveforms during power injection into the grid are demonstrated in Fig. 9. As indicated, the system injects approximately 8.5 amperes (RMS) into the utility grid at unity power factor. To analyze the harmonic content of the injected current, Fig. 10 presents its amplitude at each harmonic from the first to the twenty-fifth. It shows that the total harmonic distortion (THD) of the injected current is 9.4%. However, since the system is designed for higher current values, the harmonic distortion decreases as the system approaches its full operational point.

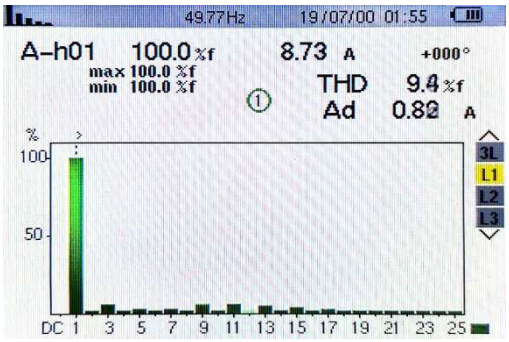

Fig. 10. Harmonic content of the grid current under uniform irradiance.

V. Conclusion

This paper presented a global characteristic scan mechanism (GCSM) designed to enhance the performance of existing local maximum power point tracking (MPPT) algorithms, such as the perturb & observe (P&O) method. The proposed mechanism focuses on minimizing the computational burden compared to other methods for identifying the global maximum power point (GMPP). In addition, its simplicity and practicality offer a distinct advantage over many other existing approaches. It is important to note that the GMPP does not appear randomly between local maxima; instead, it follows a predictable pattern, which formed the foundation of the proposed GCSM. The mechanism was implemented in a grid-tied solar inverter system and tested under various conditions, including both uniform and non-uniform irradiance.

References

[1] Elavarasan, R.M., Shafiullah, G.M., Padmanaban, S., Kumar, N.M., Annam, A., Vetrichelvan, A.M., Mihet-Popa, L. and Holm-Nielsen, J.B., 2020. A comprehensive review on renewable energy development, challenges, and policies of leading Indian states with an international perspective. *Ieee Access*, *8*, pp.74432-74457.

[2] Thipwangmek, N., Suetrong, N., Taparugssanagorn, A., Tangparitkul, S. and Promsuk, N., 2024. Enhancing Short-Term Solar Photovoltaic Power Forecasting Using a Hybrid Deep Learning Approach. *IEEE Access*.

[3] Seyedmahmoudian, M., Rahmani, R., Mekhilef, S., Oo, A.M.T., Stojcevski, A., Soon, T.K. and Ghandhari, A.S., 2015. Simulation and hardware implementation of new maximum power point tracking technique for partially shaded PV system using hybrid DEPSO method. *IEEE transactions on sustainable energy*, *6*(3), pp.850-862.

[4] Sundareswaran, K., Sankar, P., Nayak, P.S.R., Simon, S.P. and Palani, S., 2014. Enhanced energy output from a PV system under partial shaded conditions through artificial bee colony. *IEEE transactions on sustainable energy*, *6*(1), pp.198-209.

[5] Renaudineau, H., Donatantonio, F., Fontchastagner, J., Petrone, G., Spagnuolo, G., Martin, J.P. and Pierfederici, S., 2014. A PSO-based global MPPT technique for distributed PV power generation. *IEEE Transactions on Industrial Electronics*, *62*(2), pp.1047-1058.

[6] Nguyen, T.L. and Low, K.S., 2010. A global maximum power point tracking scheme employing DIRECT search algorithm for photovoltaic systems. *IEEE transactions on Industrial Electronics*, *57*(10), pp.3456-3467.

[7] Manickam, C., Raman, G.P., Raman, G.R., Ganesan, S.I. and Chilakapati, N., 2016. Fireworks enriched P&O algorithm for GMPPT and detection of partial shading in PV systems. *IEEE Transactions on Power Electronics*, *32*(6), pp.4432-4443.

[8] Mohanty, S., Subudhi, B. and Ray, P.K., 2015. A new MPPT design using grey wolf optimization technique for photovoltaic system under partial shading conditions. *IEEE Transactions on Sustainable Energy*, *7*(1), pp.181-188.

[9] Mohanty, S., Subudhi, B. and Ray, P.K., 2016. A grey wolf-assisted perturb & observe MPPT algorithm for a PV system. *IEEE transactions on energy conversion*, *32*(1), pp.340-347.

[10] Mirjalili, S., Mirjalili, S.M. and Lewis, A., 2014. Grey wolf optimizer. *Advances in engineering software*, *69*, pp.46-61.

[11] Chen, K., Tian, S., Cheng, Y. and Bai, L., 2014. An improved MPPT controller for photovoltaic system under partial shading condition. *IEEE transactions on sustainable energy*, *5*(3), pp.978-985.

[12] Tey, K.S. and Mekhilef, S., 2014. Modified incremental conductance algorithm for photovoltaic system under partial shading conditions and load variation. *IEEE Transactions on Industrial Electronics*, *61*(10), pp.5384-5392.

[13] Lei, P., Li, Y. and Seem, J.E., 2011. Sequential ESC-based global MPPT control for photovoltaic array with variable shading. *IEEE Transactions on Sustainable Energy*, *2*(3), pp.348-358.

[14] Heydari-doostabad, H., Keypour, R., Khalghani, M.R. and Khooban, M.H., 2013. A new approach in MPPT for photovoltaic array based on extremum seeking control under uniform and non-uniform irradiances. *Solar Energy*, *94*, pp.28-36.

[15] Mohapatra, A., Nayak, B., Das, P. and Mohanty, K.B., 2017. A review on MPPT techniques of PV system under partial shading condition. *Renewable and Sustainable Energy Reviews*, *80*, pp.854-867.

[16] Huynh, D.C. and Dunnigan, M.W., 2016. Development and comparison of an improved incremental conductance algorithm for tracking the MPP of a solar PV panel. *IEEE transactions on sustainable energy*, *7*(4), pp.1421-1429.

[17] Zaki, M., Shahin, A., Eskender, S. and Elsayes, M.A., 2023. Hybrid global search with enhanced INC MPPT under partial shading condition. *Scientific Reports*, *13*(1), p.22197.

[18] Alshareef, M.J., 2022. An effective falcon optimization algorithm based MPPT under partial shaded photovoltaic systems. *IEEE Access*, *10*, pp.131345-131360.

[19] Li, X., Wen, H., Hu, Y., Jiang, L. and Xiao, W., 2017. Modified beta algorithm for GMPPT and partial shading detection in photovoltaic systems. *IEEE Transactions on Power Electronics*, *33*(3), pp.2172-2186.

[20] Furtado, A.M., Bradaschia, F., Cavalcanti, M.C. and Limongi, L.R., 2017. A reduced voltage range global maximum power point tracking algorithm for photovoltaic systems under partial shading conditions. *IEEE Transactions on Industrial Electronics*, *65*(4), pp.3252-3262.